Non-uniform spacing of transverse cracks in symmetric composite laminates

Zakia Karoui, Julien Berthe, Corrado Maurini

Non-uniform spacing of transverse cracks in symmetric composite laminates

Z. Karoui[1,2], J. Berthe[2,3], C. Maurini[1,*]

May 15, 2023

Abstract We study multiple transverse cracking of symmetric laminates in the framework of the variational approach to fracture. Considering the Griffith model, we assume that several cracks can appear instantaneously through the whole thickness of the core layer, separating the bar in n elastic segments. We show that the energy minimization implies the bifurcation from solutions with uniform crack spacing to non uniformly spaced solutions, a phenomenon ignored in the literature for perfect systems. The stability of uniformly spaced solutions crucially depends on the concavity of the elastic compliance of each elastic segment as a function of the segment length. We compute this function and its derivatives numerically with domain-derivative techniques for a large set of geometric and material parameters. Our results indicate that the change of concavity and the related instability is a robust qualitative property that becomes quantitatively relevant in the case of laminates with thin and soft outer layers.

1 Introduction

Layered composite structures exhibit complex crack patterns, whose understanding is important for their engineering application. A large body of literature investigated experimentally and theoretically fracture of cross-ply fiber-reinforced composites, see the reviews of Nairn, 2000 and Berthelot, 2003. In the typical sandwich configuration, the plies composing the external layers are oriented along the load-carrying direction, say 0 degrees, and the plies in the core have fibers perpendicularly oriented, say 90 degrees. They form the so-called [0/90/0] staking sequence. The typical damage mechanisms are transverse matrix-cracking in the core, interlaminar failure in the interface between 0°/90° plies, and fiber breakage in the 0° plies.

The appearance of multiple transverse cracks in the brittle core is the predominant failure mechanism, and it is the object of the present work. The available experimental results indicate the following fundamental features: (i) cracks appear for an *in situ* stress in the core larger than the nominal strength of the standing alone lamina; (ii) the average crack spacing is decreasing

[1] CNRS, Institut Jean Le Rond d'Alembert, Sorbonne University, UMR 7190, 75005, Paris, France

[2] ONERA, Materials and Structures Department / Design & Dynamic Resistance Research Unit, 5 rue des Fortifications, CS 90013, F-59045 Lille Cedex, France

[3] Université de Lille, CNRS, Centrale Lille, UMR 9013-LaMCube, Laboratoire de Mécanique, Multiphysiques, Multiéchelles, F-59000 Lille, France

* Corresponding author, *corrado.maurini@sorbonne-universite.fr*

with the applied loading; (iii) the *in situ* strength increases when the relative core thickness decreases. Energetic fracture mechanics models predict reasonably well the *in situ* strength and the evolution of the crack spacing with the loading (Berthelot, 2003; Nairn, 2000). They assume that the cracks appear instantaneously through the whole core thickness at the center of the longest segment between two previous cracks. Their degree of accuracy depends on the hypotheses made to evaluate the elastic energy release. The available models range from basic shear-lag models (Parvizi and Bailey, 1978) to full-field finite element numerical computations, passing through sophisticated variational approximations (Berthelot et al., 1996; Hashin, 1985). The energetic models are in agreement with experiments until reaching a crack saturation regime that can be explained only by introducing additional length scales (Dvorak and Laws, 1986; García et al., 2014; Leguillon, 2002).

The existing works assume the crack distribution in the core to be either uniform, or determined by statistical criteria of defect distribution (Javaland et al., 2012; Maimí et al., 2015; Manders et al., 1983; Okabe et al., 2008; Silberschmidt, 2005; Vinogradov and Hashin, 2005). The presence of defects in initiating transverse cracks is stronger in the early stage of the multiple cracking process. Once the cracks are nearly uniformly spaced, their further multiplication is governed by the local axial stress between the cracks, whose maximum value decreases as cracks come closer. For high crack densities, the triggering of a delamination process determines a minimal possible crack spacing. (Berthelot and Corre, 2000)

In the present work, we tackle the optimal crack spacing problem within the variational approach to fracture (Francfort and Marigo, 1998) and a Griffith crack model, leveraging the ideas presented by Bourdin et al., 2008. We consider a layered composite bar n transverse cracks in the core. We show that, even in the absence of defects or imperfections, the optimal crack spacing can be non-uniform. The optimal solution of the problem depends on the concavity of the elastic compliance function of the elementary cell between two cracks, $S(\ell)$, as a function the cell length ℓ. We accurately compute the first and second derivatives of the elementary elastic compliance by the finite element method and domain-derivative techniques. Our results show that its second derivative change in sign at a critical length ℓ_c. When assuming local energy minimality as a stability criterion, the solution with uniform crack spacing is stable only when the cell length is smaller than ℓ_c. When several cracks appear simultaneously, their spacing is either homogeneous or built on two different cell lengths, a *short* and a *long* one. In analogy with the behavior of a chain of bistable springs studied by Puglisi and Truskinovsky, 2000, we show that only solutions with a single *long* cell are energetically stable.

The paper is organized as follows. Section 2 formulates the general problem of optimal crack spacing and illustrate the possible bifurcation from uniformly to non-uniformly crack spacing through direct numerical computations. Section 3 presents the modular approach, the related optimality conditions, and the numerical method for the calculation of the compliance of the basic cell and its derivative by domain derivate techniques. Section 4 discusses the basic properties of the solution of the crack spacing problem and Section 5 reports on the influence of the material and numerical parameters. Section 6 outlines standard results for calculating the optimal number of cracks. Section 7 closes the work.

2 Static variational problem for a given number of transversal cracks in the core

2.1 Problem formulation

We consider a layered composed bar of length L in Figure 1 composed of two identical outer layers of thickness H_o and a core layer of thickness H_c. We study transverse cracking in the core under the following assumptions:

- (i) the outer layers are linear elastic and unbreakable, with an elastic stiffness tensor $\mathbb{A}_o$;
- (ii) the core is perfectly brittle, being linear elastic up to fracture, with an elastic stiffness tensor $\mathbb{A}_c$ and a fracture toughness G_c.
- (iii) cracks are possible only in the core (c) and are supposed to be in the form of a finite number of $n-1$ straight cracks orthogonal to the axis of the bar and spanning the whole thickness of the core (see Figure 1);
- (iv) we assume a 2d plane-stress model in the $x-y$ plane and neglect geometric non-linearities.

Oblique cracks and delamination, usually appearing after transverse cracks in the core, are not considered here.
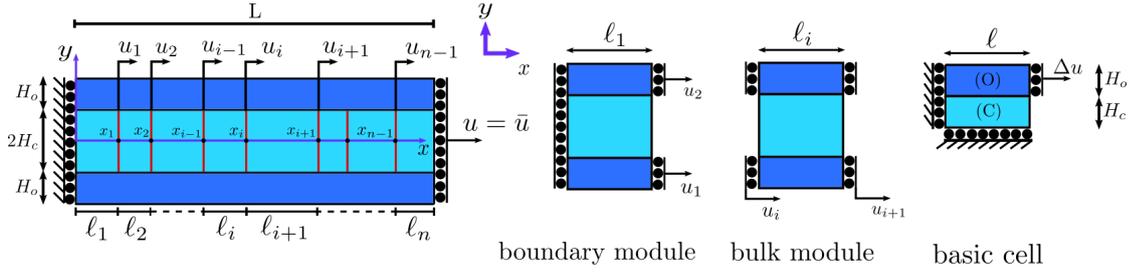

Fig. 1: Sandwich bar with $n-1$ transverse cracks in the core layer. We identify the boundary modulus, the bulk modulus, and elementary cell of the modular system.

The 2d domain $\Omega \equiv \{(x,y) \in [0,L] \times [-H_c - H_o, H_c + H_o]\}$ is the reference configuration of the solid and

$$\Gamma(\underline{\ell}) \equiv \cup_{i=1}^{n-1} \Gamma_i(\underline{\ell}) \quad \text{with} \quad \Gamma_i(\underline{\ell}) \equiv \left\{ x = \bar{x}_i := \sum_{j=1}^{i} \ell_j, \, y \in [-H_c, H_c] \right\} \tag{1}$$

is the crack set according to the assumption (iii) above, where $\bar{x}_i$ are the crack axial positions and $\underline{\ell} := \{\ell_i\}_{i=1}^{n}$ the corresponding crack spacings, see Figure 1.

We study the fracture problem in the framework of the variational approach to fracture (Bourdin et al., 2008; Francfort and Marigo, 1998), where the cracked status of the system is determined by a minimality condition on a total energy functional, sum of the elastic energy of the cracked body and the surface energy due to the cracks.

Within the Griffith fracture model, the surface energy required to create the cracks is proportional to the crack surface. For our case, the surface energy is $2(n-1)G_c H_c$. Denoting by $\mathbf{u} : \mathbf{x} = (x,y) \in \Omega \to \mathbf{u}(\mathbf{x}) \in \mathbb{R}^2$ the displacement field, the total energy functional to be minimized writes as

$$\mathcal{F}(\mathbf{u}, \underline{\ell}) := \mathcal{P}_{\text{tot}}(\mathbf{u}, \underline{\ell}) + 2(n-1)G_c H_c, \quad \mathcal{P}_{\text{tot}}(\mathbf{u}, \underline{\ell}) := \int_{\Omega \setminus \Gamma(\underline{\ell})} \frac{1}{2} \mathbb{A}(\mathbf{x}) \varepsilon(\mathbf{u}(\mathbf{x})) \cdot \varepsilon(\mathbf{u}(\mathbf{x})) \, d\mathbf{x}, \tag{2}$$

where the first term is the elastic energy of the cracked solid, $\varepsilon(\mathbf{u}) := \text{sym}(\nabla \mathbf{u})$ being the linearized strain tensor. We consider the general case of orthotropic constituent materials under plane-stress condition, for which, using the Voigt notation:

$$\mathbb{A}_{m \in \{o,c\}} = \frac{1}{1 - \nu_m^{xy} \nu_m^{yx}} \begin{bmatrix} E_m^x & E_m^x \nu_m^{yx} & 0 \\ E_m^y \nu_m^{xy} & E_m^y & 0 \\ 0 & 0 & (1 - \nu_m^{xy} \nu_m^{yx}) G_m^{xy} \end{bmatrix}, \qquad \varepsilon(\mathbf{u}) = \begin{bmatrix} \frac{\partial u_x}{\partial x} \\ \frac{\partial u_y}{\partial y} \\ \left(\frac{\partial u_x}{\partial y} + \frac{\partial u_y}{\partial x} \right) \end{bmatrix}. \tag{3}$$

For isotropic materials with Young modulus E_m and Poisson ratio ν, $E_m^x = E_m^y = E_m$, $\nu_m^{yx} = \nu_m^{xy} = \nu_m$, and $G_m^{xy} = E_m/(2(1+\nu_m))$.

We assume that the bar is loaded in traction by a hard device imposing a vanishing axial displacement on the left-end side and the axial displacement $\bar{u}$ on the right-end side. The space of admissible displacement field $\mathcal{C}_{\bar{u}}$ must respect these Dirichlet boundary conditions and should be regular except on the cracks, where it can jump, namely

$$\mathcal{C}_{\bar{u}}(\underline{\ell}) = \{\mathbf{u} \in \mathsf{H}^1(\Omega \setminus \Gamma): \quad u_1(0,x_2) = 0, \, u_1(L,x_2) = \bar{u}, \, \forall x_2 \in [-H_c - H_o, H_c + H_o]\}, \quad (4)$$

where $\mathsf{H}^1(\Omega, \mathbb{R}^2)$ is the usual Sobolev space of functions with square integrable first derivatives defined on Ω and with values in $\mathbb{R}^2$.

We apply here the variational approach to fracture (Bourdin et al., 2008), to determine the crack spacings $\underline{\ell}$'s for a given loading and number of cracks $n-1$. We will discuss only briefly in Section 6 how to determine the optimal number of cracks as a function of the loading.

2.2 The static variational problem

We denote as the *static problem* the determination of the cracked state of the solid for a fixed loading (here the imposed displacement $\bar{u}$). In the static problem, we ignore any history effect and irreversibility condition on the evolution of the cracks.

Adopting the variational approach to fracture and the hypotheses above, this problem consists in solving the following minimization problem for the total energy functional (2):

$$\min_{\mathbf{u},\underline{\ell},n}\{\mathcal{F}(\mathbf{u},\underline{\ell}), \quad \text{with} \quad \mathbf{u} \in \mathcal{C}_{\bar{u}}(\underline{\ell}), \quad \underline{\ell} \in \mathbb{R}^n, \quad \sum_{i=1}^n \ell_i = L, \quad n \in \mathbb{N}\}. \quad (5)$$

Differently from previous works (Berthelot, 2003; Nairn, 2000), we do not assume any hypothesis on the crack spacings, neither we introduce statistical distribution of defects that can influence the fracture toughness or the energy release associated with a crack.

Thanks to the hypothesis of linear elastic behavior in $\Omega \setminus \Gamma$, we can uniquely determine the displacement field and the corresponding elastic energy as a function of the crack spacings $\underline{\ell}$, as follows:

$$\mathbf{u}^*(\underline{\ell}) = \mathrm{argmin}\{\mathcal{P}_{\mathrm{tot}}(\mathbf{u},\underline{\ell}), \quad \mathbf{u} \in \mathcal{C}_{\bar{u}}(\underline{\ell})\}, \quad \mathsf{P}_{\mathrm{tot}}(\underline{\ell}) = \mathcal{P}_{\mathrm{tot}}(\mathbf{u}^*(\underline{\ell}),\underline{\ell}). \quad (6)$$

Hence, the variational problem (5) can be reduced to the following constrained optimization problem in $\mathbb{R}^n$:

$$\min_{\underline{\ell},n}\left\{\mathsf{F}(\underline{\ell}), \quad \underline{\ell} \in \mathbb{R}^n, \quad \sum_{i=1}^n \ell_i = L, \quad n \in \mathbb{N}\right\}, \quad \text{with} \quad \mathsf{F}(\underline{\ell}) := \mathsf{P}_{\mathrm{tot}}(\underline{\ell}) + 2\,(n-1)\,G_c\,H_c. \quad (7)$$

As far as the number of cracks $n-1$ is given, the surface energy is fixed, being independent of the crack spacing. Hence, the key problem is to find the optimal spacing $\underline{\ell}$ to minimize the elastic energy $P_{\mathrm{tot}}(\underline{\ell})$.
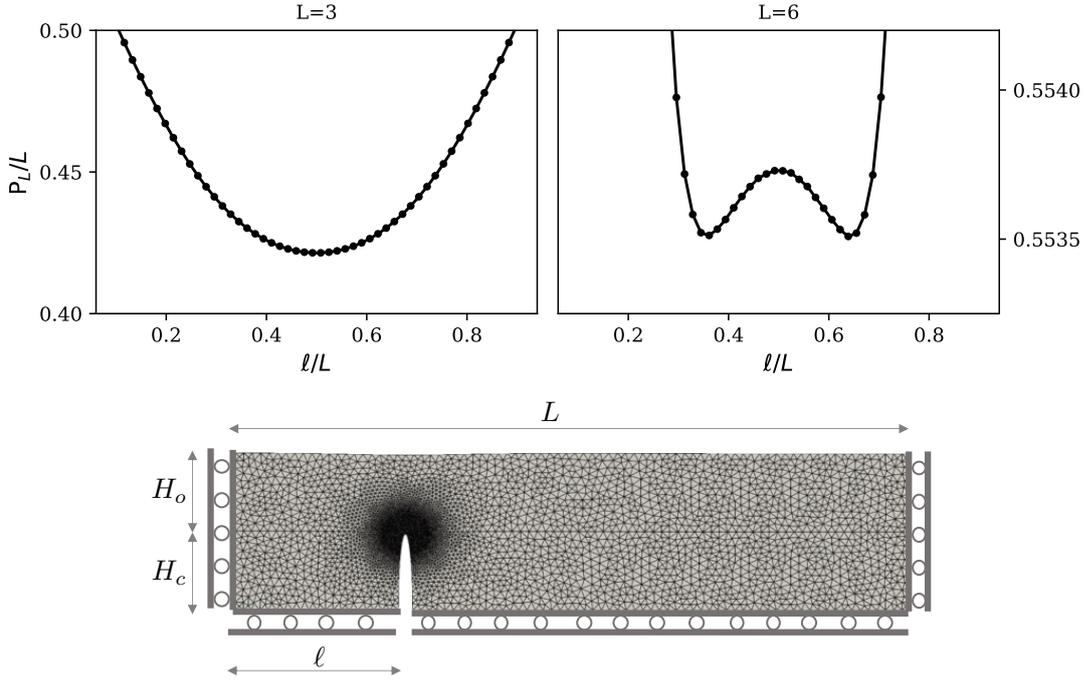
Fig. 2: Top: potential energy of the composite bar with a single crack as a function of the crack position ℓ for different bar lengths L; each point in the graphs corresponds to a finite element computation. Bottom: a typical mesh deformed using the displacement solution of the problem) and boundary conditions. For short bars ($L = 3$) there is a single minimum corresponding to the optimal crack position $\ell = L/2$ breaking the bar in two segments of equal length. For long bars ($L = 6$), $\ell = L/2$ becomes a maximum, with two new minima for $\ell = L/2 \pm \Delta\ell$, suggesting a pitchfork bifurcation. The numerical results are for $E_o = E_c = 1$, $H_c = 1$, $H_o = 0.5$, $\nu_c = \nu_o = 0.3$.

2.3 An example of solutions with non-uniform spacing: a bar with a single crack

Let us consider the simple example of a bar of length L with a single crack in the core layer, splitting it in two segments of length $\ell_1 = \ell$ and $\ell_2 = L - \ell$, as shown in Figure 2. For this case, the variational problem (7) reduces to

$$\min_{0<\ell<L} \mathsf{P}_L(\ell) = \mathsf{P}_{tot}(\ell, \ell - L). \tag{8}$$

For a given bar length L and crack spacing ℓ, we compute the elastic energy $\mathsf{P}_L(\ell)$ by solving the linear elastic problem (6). We use a standard finite element approach with an unstructured uniform mesh and the geometry shown in Figure 2. Figure 2 reports two typical plots of the potential energy $\mathsf{P}_L(\ell)$ as a function of the crack position ℓ. The computations are for isotropic layers with Young moduli ratio $E_o/E_c = 1$, Poisson's coefficients $\nu_c = \nu_o = 0.3$, and thickness ratio $H_o/H_c = 0.5$. We observe two different regimes :

– For short bars ($L/H_c = 3$) the elastic energy has a single minimum at $\ell^* = L/2$, corresponding to a crack dividing the bar in two segments of equal length.

– For long bars ($L/H_c = 6$), the elastic energy has two minima at $\ell_1^*, \ell_2^* = L - \ell_1^*$, corresponding to a crack dividing the bar in a short and a longer segment.

This simple example shows that the problem of the optimal crack spacing is non-trivial. Solutions with uniform spacing can be energetically unstable for sufficiently long bars. The commonly accepted assumption (see e.g. Berthelot, 2003; Nairn, 2000) that the optimal crack position is at the center of the bar is not always in agreement with the energy minimality criterion: for sufficiently long bars the optimal crack spacing can be non-uniform, even in perfect systems. This observation calls for a more general analysis to better understand the case with several cracks and to investigate the dependence on the material and geometric parameters.

3 Modular energetic approach for the case with several cracks

When considering a bar with several cracks, calculating the function $P_{\text{tot}}(\underline{\ell})$ requires solving the linear elasticity problem (6) for each combination of spacing $\underline{\ell}$. A direct numerical strategy is not practical for more than one crack. To unveil the key property of the solution, we develop a modular approach and write the elastic energy of the system in terms of the elastic compliance of an elementary cell.

3.1 The elastic energy as a function of the crack spacing

We regard the cracked beam as modular system composed of the boundary and bulk modules sketched in Figure 1. This decomposition requires the axial displacement to be constant throughout the outer layers in the cracked cross-sections, a mild assumption that is closely verified in practice. Let us denote by u_i the displacement for the cross section $x = \bar{x}_i$ of the crack Γ_i and by $\Delta u_i = u_{i+1} - u_i$ the elongation imposed to the i-th cell of length ℓ_i. Exploiting the symmetries, both modules are a special arrangements of the basic cell in Figure 1. By the linearity of the problem, the elastic energy of the elementary cell of length ℓ is quadratic with respect to the imposed elongation Δu and can be written in the form

$$P_{\text{cell}}(\ell) = \frac{1}{2} \mathsf{K}(\ell) \, \Delta u^2, \tag{9}$$

where the scalar valued function $\mathsf{K}(\ell)$ is the global stiffness of the elementary cell. The function $\mathsf{K}(\ell)$ can be calculated by solving an elementary cell problem, as it will be discussed in the next section. Because of the symmetries, the potential energy of the boundary and bulk cells in Figure 1 are then given by

$$P_1(\ell) = 2 \, \mathsf{K}(\ell) \, \frac{\Delta u_1^2}{2}, \quad P_n(\ell) = 2 \, \mathsf{K}(\ell) \, \frac{\Delta u_n^2}{2}, \quad P_i(\ell) = 4 \, \mathsf{K}(\ell/2) \, \frac{(\Delta u_i/2)^2}{2} \text{ for } i = 2, \dots, n-1.$$

For the cell at the boundaries, it is sufficient to multiply by two the energy of the elementary cell, whilst for the energy of a bulk modulus of lenght ℓ_i and applied elongation Δu_i is four times the energy of elementary cell of length $\ell_i/2$ with an applied elongation $\Delta u = \Delta u_i/2$. Hence, the total energy of the composite bar as a function of the segment lengths and elongations writes as:

$$\mathsf{P}_{\text{tot}}(\underline{\ell}; \underline{\Delta u}) = \mathsf{K}(\ell_1) \, \Delta u_1^2 + \mathsf{K}(\ell_n) \, \Delta u_n^2 + \sum_{i=2}^{n-1} \frac{1}{2} \, \mathsf{K}(\ell_i/2) \, \Delta u_i^2. \tag{10}$$

The optimal elongation of the segments to approach the solution of the problem (6) can be determined by minimizing $\mathsf{P}_{\mathrm{tot}}(\underline{\ell}; \underline{\Delta u})$ under the constraint $\sum_{i=1}^{n} \Delta u_i = \bar{u}$. This gives the following first-order optimality conditions, see e.g. Luenberger, 2008:

$$\Delta u_1 = \frac{F}{2\,\mathsf{K}(\ell_1)}, \quad \Delta u_i = \frac{F}{\mathsf{K}(\ell_i/2)} \text{ for } i = 2, \ldots, n-1, \quad \Delta u_n = \frac{F}{2\,\mathsf{K}(\ell_n)}, \quad \sum_{i=1}^{n} \Delta u_i = \bar{u},$$

where F is the Lagrange multiplier representing the total reaction force acting on the bar to impose the end-displacement. After elementary algebraic manipulations, one finds the following final expression for the total elastic energy as a function of the crack spacing:

$$\mathsf{P}_{\mathrm{tot}}(\underline{\ell}) = \mathsf{K}_{\mathrm{tot}}(\underline{\ell})\,\frac{\bar{u}^2}{2} = \frac{1}{\mathsf{S}_{\mathrm{tot}}(\underline{\ell})}\frac{\bar{u}^2}{2}, \tag{11}$$

where

$$\mathsf{S}_{\mathrm{tot}}(\underline{\ell}) = \frac{\mathsf{S}(\ell_1)}{2} + \sum_{i=2}^{n-1} \mathsf{S}(\ell_i/2) + \frac{\mathsf{S}(\ell_n)}{2}, \quad \mathsf{K}_{\mathrm{tot}}(\underline{\ell}) = \frac{1}{\mathsf{S}_{\mathrm{tot}}(\underline{\ell})}, \tag{12}$$

are the equivalent total compliance and stiffness of the composite bar and

$$\mathsf{S}(\ell) = \frac{1}{\mathsf{K}(\ell)} = \frac{\Delta u^2}{2\mathsf{P}_{\mathrm{cell}}(\ell)} \tag{13}$$

is the compliance of the elementary cell, the fundamental brick of our approach.

3.2 The optimal crack spacing problem

The optimal crack spacing is given by the solution of the problem (7), which reduces to the minimization of the elastic energy $\mathsf{P}_{\mathrm{tot}}(\underline{\ell})$ under the constraint $\sum_{i=1}^{n} \ell_i = L$. Using the expression (11), this can be recast as the following maximization problem for the total elastic compliance (12):

$$\max_{\underline{\ell}} \left\{ \mathsf{S}_{\mathrm{tot}}(\underline{\ell}), \quad \underline{\ell} \in \mathbb{R}^n, \quad \sum_{i=1}^{n} \ell_i = L \right\} \tag{14}$$

Eliminating the constraint by setting $\ell_n = L - \sum_{i=1}^{n-1} \ell_i$, gives an unconstrained maximisation problem in $\mathbb{R}^{n-1}$. A solution $\{\ell_i^*\}_{i=1}^{n-1}$ must verify the following first order optimality conditions:

$$\left\{ \frac{\partial \mathsf{S}_{\mathrm{tot}}(\ell_1^*, \ell_{n-1}^*, L - \sum_{i=1}^{n-1}\ell_i)}{\partial \ell_i} = 0 \right\}_{i=1}^{n-1} \Leftrightarrow \begin{cases} \mathsf{S}'(\ell_1^*) = \mathsf{S}'(L - \sum_{i=1}^{n-1}\ell_i^*), \\ \mathsf{S}'(\ell_i^*/2) = \mathsf{S}'(L - \sum_{i=1}^{n-1}\ell_i^*) & \text{for } i = 2, \ldots, n-1. \end{cases} \tag{15}$$

Second-order optimality conditions are given by the sign of the $(n-1) \times (n-1)$ Hessian matrix H of second derivatives, which is calculated to get:

$$\mathsf{H} = \frac{1}{2}\begin{bmatrix} \mathsf{H}_1 + \mathsf{H}_n & \mathsf{H}_n & \ldots & \mathsf{H}_n \\ \mathsf{H}_n & \mathsf{H}_2 + \mathsf{H}_n & \ldots & \mathsf{H}_n \\ \ldots & \ldots & \ldots & \ldots \\ \mathsf{H}_n & \mathsf{H}_n & \ldots & \mathsf{H}_{n-1} + \mathsf{H}_n \end{bmatrix}, \quad \text{with} \quad \begin{cases} \mathsf{H}_1 = \mathsf{S}''(\ell_1^*) \\ \mathsf{H}_i = \mathsf{S}''(\ell_i^*/2)/2, & i = 2, \ldots, n-1 \\ \mathsf{H}_n = \mathsf{S}''(L - \sum_1^{n-1}\ell_i^*) \end{cases} \tag{16}$$

The sign of the Hessian matrix determines the stability of the solution: if the Hessian matrix evaluated at a given solution is negative definite, the solution is stable, being a maximizer of the
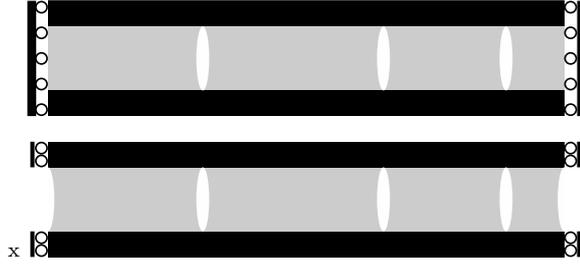
Fig. 3: Composite bar with alternative with the diplacement imposed only on the outer layer. In this case, differently from the case in Figure 1 there is no need for a distinction between boundary modules and bulk modules. All the modules are of the bulk type of Figure 1, see also Remark 1.

total compliance, hence a minimizer of the total potential energy. Vice-versa, if it is not negative semi-definite, the solution is unstable. The Hessian matrix happens to be in the same form as the one of the chain of bistable springs studied by Puglisi and Truskinovsky, 2000. We apply here the results of their stability analysis:

(S1) If $\mathsf{H}_i < 0$ for all $i = 1, \dots, n$, then the matrix is negative definite and the solution is stable.
(S2) If there are two or more than $\mathsf{H}_i > 0$, the matrix has at least one positive eigenvalue and the solution is unstable.
(S3) If only one of the H_i is positive and $n - 1$ are negative, the solution is stable if

$$r := \sum_{i=1}^{n} \frac{1}{\mathsf{H}_i} < 0 \tag{17}$$

and unstable if the same quantity is $r > 0$.

A trivial solution of the problem (15) is the solution with uniform spacings, for which

$$\ell_1 = \ell_n = \ell^*, \quad \ell_i = 2\ell^*, \quad \text{with} \quad \ell^* = \frac{L}{2\,(n-1)}. \tag{18}$$

This solution exists independently of the property of the function $\mathsf{S}'(\ell^*)$. However, the Hessian matrix (16) is negative definite only if $\mathsf{S}''(\ell^*) \leq 0$. The solution with uniform spacing is stable only if $\mathsf{S}''(\ell^*) \leq 0$.

Solutions with non-uniform spacings for (15) require that the existence of cell lengths $\ell_I^* > 0$ and $\ell_{II}^* > \ell_I^*$ such that $\mathsf{S}'(\ell_I^*) = \mathsf{S}'(\ell_{II}^*)$. To assess whether this is possible, we need first to compute the function $\mathsf{S}'(\ell^*)$ and $\mathsf{S}''(\ell^*)$ and determine their qualitative properties.

Remark 1 A simpler variant of the problem is obtained by considering the case where only the displacement of the upper layer is imposed at the two ends, as shown in Figure 3. In that case, there are no special boundary modules and the total compliance (12) reduces to:

$$\mathsf{S}_{\text{tot}}(\underline{\ell}) = \sum_{i=1}^{n} \mathsf{S}(\ell_i/2). \tag{19}$$

3.3 Elementary cell problem: computing the elastic compliance of the elementary cell and its derivatives

The modular approach defines the total elastic energy of a bar with several cracks as a function of the elastic energy of the elementary cell in Figure 1. The solution of the optimization problem (14) requires the accurate computation of the compliance (13) of the elementary cell $\mathsf{S}(\ell)$ as a function of its length and of its first and second derivatives $\mathsf{S}'(\ell)$, $\mathsf{S}''(\ell)$. We compute these functions through a domain-derivative approach and by solving the elementary cell problem through a classical finite element method.

To accurately evaluate the derivatives of $\mathsf{S}(\ell)$ with respect to the domain length, we reformulate the elastic cell problem for a cell of length ℓ on a ℓ-independent domain $\widetilde{\Omega} \equiv \widetilde{\Omega}_c \cup \widetilde{\Omega}_o$ of length $\tilde{\ell}$ by performing the following change of coordinates

$$\mathbf{x} = (x, y) \in \Omega_\ell \to \widetilde{\mathbf{x}} = (\widetilde{x}, \widetilde{y}) \in \widetilde{\Omega} \quad \text{with} \quad \widetilde{x} = \frac{\widetilde{\ell}}{\ell}\, x, \quad \widetilde{y} = y, \tag{20}$$

for which

$$\frac{\partial(\cdot)}{\partial x} = \frac{\widetilde{\ell}}{\ell}\frac{\partial(\cdot)}{\partial\widetilde{x}}, \quad \frac{\partial(\cdot)}{\partial y} = \frac{\partial(\cdot)}{\partial\widetilde{y}}.$$

This change of coordinate defines a new energy density

$$\widetilde{W}_\ell(\mathbf{u}) = \frac{1}{2}\frac{\ell}{\widetilde{\ell}}\, \mathbb{A}(\mathbf{x})\tilde{\varepsilon}(\mathbf{u}(\mathbf{x})) \cdot \tilde{\varepsilon}(\mathbf{u}(\mathbf{x}))$$

on the fixed domain $\tilde{\Omega}$ such that:

$$\mathcal{P}_\ell(\mathbf{u}) := \int_{\Omega_\ell} \frac{1}{2}\mathbb{A}(\mathbf{x})\varepsilon(\mathbf{u}(\mathbf{x})) \cdot \varepsilon(\mathbf{u}(\mathbf{x}))\, \mathrm{d}\mathbf{x} = \int_{\widetilde{\Omega}} \widetilde{W}_\ell(\mathbf{u})\, \mathrm{d}\widetilde{\mathbf{x}},$$

where

$$\tilde{\varepsilon}(\mathbf{u}) = \left[\frac{\tilde{\ell}}{\ell}\frac{\partial u_x}{\partial\widetilde{x}},\ \frac{\partial u_y}{\partial\widetilde{y}},\ \left(\frac{\partial u_x}{\partial\widetilde{y}} + \frac{\tilde{\ell}}{\ell}\frac{\partial u_y}{\partial\widetilde{x}}\right)\right]^T.$$

The solution of the following minimization problem on the ℓ-independent domain gives the elastic energy of the cell:

$$\mathbf{u}_\ell := \underset{\mathbf{u}\in\widetilde{\mathcal{C}}}{\operatorname{argmin}}\, \mathcal{P}_\ell(\mathbf{u}), \qquad \mathsf{P}_{\mathrm{cell}}(\ell) = \mathcal{P}_\ell(\mathbf{u}_\ell), \tag{21}$$

where the space of admissible displacements includes the Dirichlet boundary conditions

$$\widetilde{\mathcal{C}} = \{\mathbf{u} \in \mathsf{H}^1(\widetilde{\Omega}) :\ u_1(0, \widetilde{x}_2 \in [0, H_c + H_o]) = u_2(\widetilde{x}_1 \in [0, \widetilde{\ell}], 0) = 0,$$
$$u_1(\widetilde{\ell}, \widetilde{x}_2 \in [H_c, H_c + H_o]) = \Delta u\}. \tag{22}$$

The first order optimality condition for (21) gives the linear system to solve, a standard linear elastic problem on the unit cell:

$$\mathcal{D}\mathcal{P}_\ell(\mathbf{u}_\ell)[\mathbf{v}] = 0, \quad \forall \mathbf{v} \in \widetilde{\mathcal{C}}_0. \tag{23}$$

Here and henceforth, we denote by

$$\mathcal{D}\mathcal{F}(\mathbf{u})[\mathbf{v}] := \frac{d}{dh}\mathcal{F}(\mathbf{u} + h\,\mathbf{v})\bigg|_{h=0}, \quad \mathcal{D}^2\mathcal{F}(\mathbf{u})[\mathbf{w}, \mathbf{v}] := \frac{d}{dh}\mathcal{D}\mathcal{F}(\mathbf{u} + h\,\mathbf{w})[\mathbf{v}]\bigg|_{h=0} \tag{24}$$
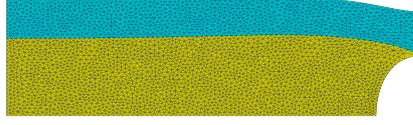
Fig. 4: Typical finite element mesh in the deformed configuration used for the computation of the basic cell compliance $S(\ell)$ for $H_c = 1$, $H_o = 0.5$, $L = 4$ (outer layer in cyan and core layer in yellow).

the first and second directional derivative of the functional $\mathcal{F}$ with respect to $\mathbf{u}$ in the directions $\mathbf{v}$ and $\mathbf{w}$ and by $\widetilde{\mathcal{C}}_0$ the space of admissible variations associated to $\widetilde{\mathcal{C}}$.

With the change of coordinate (20), the cell length ℓ appears directly as a parameter in the energy. Hence, the domain derivatives can be straightforwardly computed as

$$\mathsf{P}'_{\text{cell}}(\ell) := \frac{d\mathsf{P}_{\text{cell}}(\ell)}{d\ell} = \dot{\mathcal{P}}_\ell(\mathbf{u}_\ell) + \cancelto{0}{\mathcal{DP}_\ell(\mathbf{u}_\ell)[\dot{\mathbf{u}}_\ell]} = \dot{\mathcal{P}}_\ell(\mathbf{u}_\ell),\tag{25a}$$

$$\mathsf{P}''_{\text{cell}}(\ell) := \frac{d^2\mathsf{P}_{\text{cell}}(\ell)}{d\ell^2} = \ddot{\mathcal{P}}_\ell(\mathbf{u}_\ell) + \mathcal{D}\dot{\mathcal{P}}_\ell(\mathbf{u}_\ell)[\dot{\mathbf{u}}_\ell]\tag{25b}$$

where

$$\dot{\mathcal{P}}_\ell(\mathbf{u}) := \int_{\widetilde{\Omega}} \frac{\partial \widetilde{W}_\ell}{\partial \ell}(\mathbf{u})\,d\widetilde{\mathbf{x}}, \quad \ddot{\mathcal{P}}_\ell(\mathbf{u}) := \int_{\widetilde{\Omega}} \frac{\partial^2 \widetilde{W}_\ell}{\partial \ell^2}(\mathbf{u})\,d\widetilde{\mathbf{x}}.$$

and $\dot{\mathbf{u}}_\ell$ is derivative of the solution with respect to ℓ. The computation of the first derivative does not require the knowledge of $\dot{\mathbf{u}}_\ell$ because the second term in (25a) is equal to zero thanks to the stationarity condition (23). Vice-versa, the evaluation of the second derivative requires the sensitivity of the solution with respect to the cell length $\dot{\mathbf{u}}_\ell$. Taking the derivative with respect to ℓ of the weak form of the equilibrium condition (23) gives the following linear tangent problem to solve for $\dot{\mathbf{u}}_\ell$:

$$\dot{\mathbf{u}}_\ell \in \widetilde{\mathcal{C}}_0: \quad \mathcal{D}^2\mathcal{P}_\ell(\mathbf{u}_\ell)[\dot{\mathbf{u}}_\ell, \mathbf{v}] + \mathcal{D}\dot{\mathcal{P}}_\ell(\mathbf{u}_\ell)[\mathbf{v}] = 0, \quad \forall \mathbf{v} \in \widetilde{\mathcal{C}}_0.\tag{26}$$

Using these results, we evaluate $\mathsf{S}(\ell), \mathsf{S}'(\ell), \mathsf{S}''(\ell)$ for given material parameters and geometry with a standard finite-element technique as follows:

1. Mesh the fictitious domain with a unstructured triangular mesh. A tipical mesh is shown in Figure 5.

2. Solve the linear elastic problem (23) on the fictitious domain to get $\mathbf{u}_\ell$ for $\Delta u = 1$ and evaluate $\mathsf{S}(\ell) = 2/\mathsf{P}_{\text{cell}}(\ell)$ and $\mathsf{S}'(\ell) = -2\,\mathsf{P}'_{\text{cell}}(\ell)/\mathsf{P}^2_{\text{cell}}(\ell)$ with $\mathsf{P}_{\text{cell}}(\ell) = \mathcal{P}_\ell(\mathbf{u}_\ell)$ and $\mathsf{P}'_{\text{cell}}(\ell) = \dot{\mathcal{P}}_\ell(\mathbf{u}_\ell)$.

3. Solve the linear tangent problem (26) on the fictitious domain to get $\dot{\mathbf{u}}_\ell$ and evaluate $\mathsf{S}''(\ell) = -2\mathsf{P}'_{\text{cell}}(\ell)^2/\mathsf{P}^2_{\text{cell}}(\ell) + 2\mathsf{P}''_{\text{cell}}(\ell)/\mathsf{P}_{\text{cell}}(\ell)$ with $\mathsf{P}''_{\text{cell}}(\ell)$ given by (25b).

In practice the linear problems (23) and (26) are solved using the finite element library `FEniCSx` (Scroggs et al., 2022) and the derivatives implied in their expressions are computed automatically exploiting the automatic symbolic differential capabilities of the `UFL` package (Alnæs et al., 2014).

Figure 5 reports the graph of $\mathsf{P}'_{\text{cell}}(\ell)$, $\mathsf{S}'(\ell)$ and $\mathsf{S}''(\ell)$ as a function of the cell length ℓ for a bar made of isotropic materials with $E_o/E_c = 1$, $H_o/H_c = 0.5$, $\nu = 0.3$, as for the example
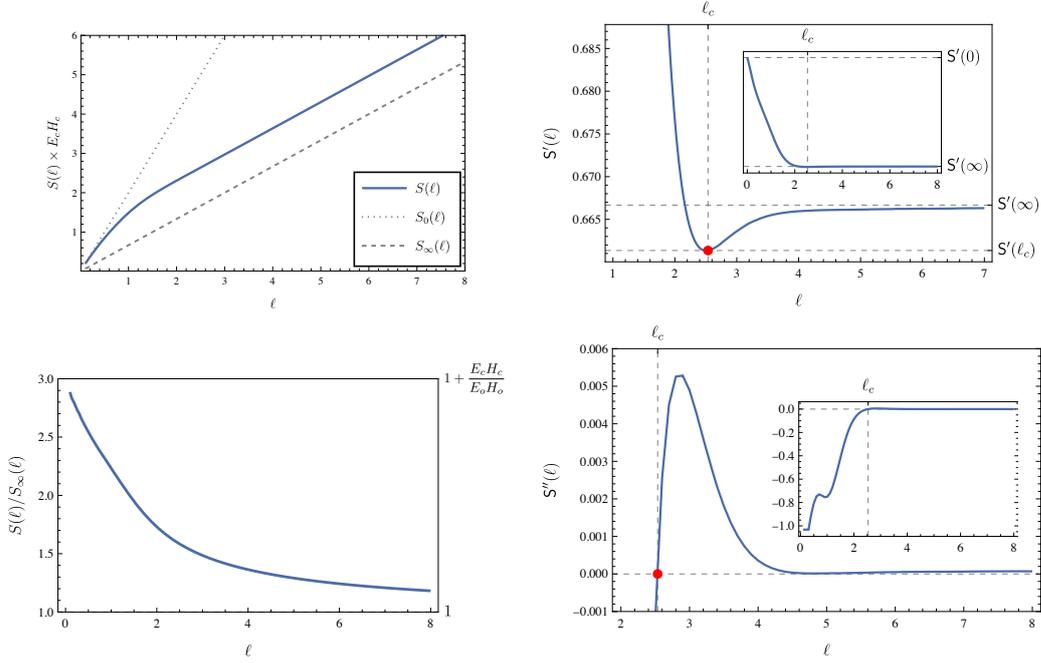
Fig. 5: First and second derivative of the compliance $S(\ell)$ for a composite bar made of isotropic materials with $E_o/E_c = 1$, $H_o/H_c = 0.5$, $\nu = 0.3$. The numerical results are for a domain with $H_c = 1$. Here and henceforth, all the lengths should be regarded as non-dimensional with respect to the scaling length H_c, which is not reported explicitly in the plot labels.

in Figure 2. These curves are the result of the interpolation of 100 data points corresponding to finite element simulations for uniformly spaced cell lengths $\ell \in [0.1, 10]$. In our numerical experiments, we observed that the qualitative behavior of these functions do not depend on the specific value of the thicknesses and Young modulus ratio (see the following Section 5). Their key properties are:

(P1) For $\ell \to 0$ one can neglect the influence of the core layer, getting the following limit elastic energy and compliance:

$$\mathsf{P}_0(\ell) = \frac{E_o^x H_o}{\ell} \frac{\Delta u^2}{2}, \qquad \mathsf{S}_0(\ell) = \frac{\ell}{(E_o^x H_o)}. \tag{27}$$

(P2) for $\ell \to \infty$ the solution of the problem (23) is given by the classical laminate theory. The only non-vanishing component of the stress is the axial stress σ_{xx}, being equal to $E_c^x \Delta u/\ell$ in the core and $E_o^x \Delta u/\ell$ in the outer layer. This gives the following elastic energy and compliance:

$$\mathsf{P}_\infty(\ell) = \frac{E_c^x H_c + E_o^x H_o}{\ell} \frac{\Delta u^2}{2}, \qquad \mathsf{S}_\infty(\ell) = \frac{\ell}{E_c^x H_c + E_o^x H_o} \tag{28}$$

(P3) There exist a finite critical cell length ℓ_c such that the derivative of the compliance, $\mathsf{S}'(\ell)$, is monotonically decreasing for $\ell \in (0, \ell_c)$, where $\mathsf{S}'(\ell) < 0$, and monotonically increasing for $\ell > \ell_c$, where $\mathsf{S}'(\ell) > 0$. The cell length for which the compliance attains its minimal value is the solution of $\mathsf{S}''(\ell_c) = 0$.
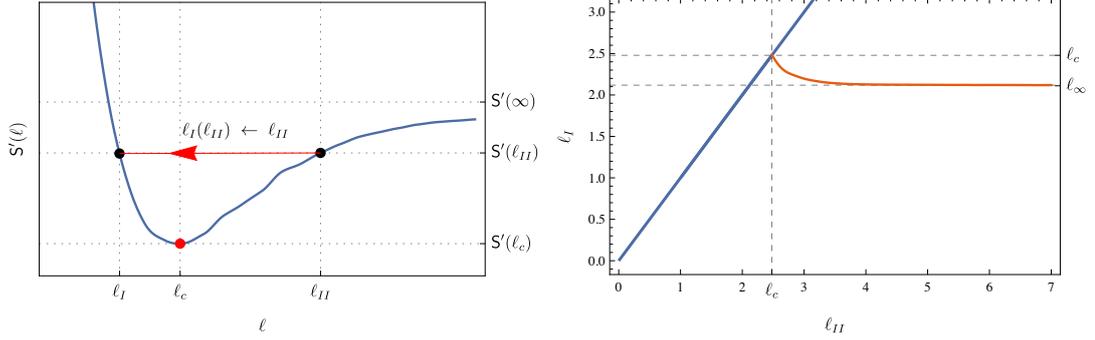
Fig. 6: Length of short segment ℓ_I as a function of the length of the long segment ℓ_{II}. Left: graphical illustration of the problem of finding $\ell_I < \ell_c$ such that $S'(\ell_I) = S'(\ell_{II})$ given $\ell_{II} > \ell_c$. Right: resulting function $\ell_I(\ell_{II})$, showing also the trivial solution $\ell_I = \ell_{II}$, in blue.
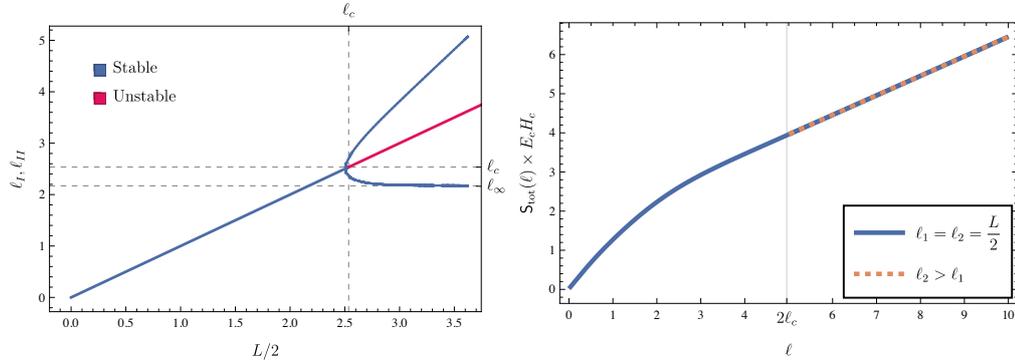

Fig. 7: Solution for a bar divided in a short and long segment by a single crack ($n = 2$). Left: lengths of the short (ℓ_I) and long segment (ℓ_{II}) as a function of the total bar length L with stable solution marked in blue and unstable solutions in pink. Right: Total elastic compliance of the homogeneous solution and the solution with two different segment lengths. Results for $E_o/E_c = 1$, $H_o/H_c = 0.5$.

In our numerical experiments, we observed that these key properties stay true for a wide range of material and geometric parameters. We will discuss in Section 5 the dependence of ℓ_c on the stiffness ratio and the thickness ratio.

4 Solutions for the crack spacing problem and their stability.

4.1 The case of one crack diving the bar in two segments

We revisit here at the light of our analysis the results anticipated in Section 2.3 for a bar divided in two sub-segments by a single crack. This is the simplest case, but also the most important. The previous works on composite cracking (see e.g. Berthelot, 2003; Nairn, 2000) commonly assume that no more than one crack can appear simultaneously. In absence of imperfections, their n-crack solution is the result of an evolution process with a cascade of cracking events breaking

the longest segment in two equal parts. We study the competition between the homogeneous solution with equal segment lengths $\ell_1 = \ell_2 = L/2$ and solutions with $\ell_1 \neq \ell_2$.

For $n = 2$, the system (15) of first order optimality conditions for the crack spacing problem (7) reduces to the condition $\mathsf{S}'(\ell_1) = \mathsf{S}'(\ell_2)$. When the properties (P1-P3) of Section 3.3 are verified, there can be at most two distinct cell lengths ℓ_I and $\ell_{II} > \ell_I$ such that $\mathsf{S}'(\ell_I) = \mathsf{S}'(\ell_{II})$. For each $\ell_{II} > \ell_c$ there exists a unique $\ell_I(\ell_{II}) < \ell_c$ solution of $\mathsf{S}'(\ell_I) = \mathsf{S}'(\ell_{II})$. Figure 6 illustrates the problem graphically (left) and reports the corresponding function $\ell_I(\ell_{II})$ (right). To compute it, we construct an interpolating function from the data of $S'(\ell)$ coming from the finite element computations of Section 3.3, we solve the nonlinear equation numerically for a set of given ℓ_{II}, and tabulate the interpolating function for $\ell_I(\ell_{II})$ once for all. When looking for ℓ_I given ℓ_{II}, the numerical root-finding procedure converges robustly even in presence of the small scale oscillations of the finite element results, as those visible in the plot of Figure 6-left. Vice-versa, the complementary approach of finding the long segment given the short one leads to hill-conditioned problems and must be avoided. As clear from the graphical illustration of Figure 6-left and the properties (P1-P3) of Section 3.3, the function $\ell_I(\ell_{II})$ monotonically decreases from ℓ_c to the asymptotic value $\ell_\infty := \ell_I(\infty)$.

To solve the crack spacing problem, it remains to determine the segment lengths $\ell_I(L)$ and $\ell_{II}(L)$ as a function of the total bar length L such that $L = \ell_I(L) + \ell_{II}(L)$. Given $\ell_I(\ell_{II})$, this is easily obtained by solving numerically a root finding problem, which has a unique solution for $\ell_{II} > \ell_c$. Finally, we get the diagram in Figure 7-left, showing a bifurcation from the fundamental homogeneous solution $\ell_I = \ell_{II}$ to the solution with $\ell_{II} > \ell_I$. Stable solutions are in blue and unstable solutions in pink, where the stability is tested with the second-order condition of Section 3.2. For $n = 2$ the latter simplifies to $S''(\ell_{II}) < -S''(\ell_I)$. We can summarize the results for a single crack as follows:

– The homogeneous solution with equal segment lengths $\ell_1 = \ell_2 = L/2$ is stable for $L < 2\ell_c$ and unstable for $L > 2\ell_c$. The corresponding total compliance of the bar is

$$\mathsf{S}_{\mathrm{tot}}(L) = \mathsf{S}_{\mathrm{tot}}(L/2). \tag{29}$$

– For $L > 2\ell_c$ there are two energetically equivalent stable solutions with $\ell_1 = \ell_I$ and $\ell_2 = \ell_{II}$ or $\ell_1 = \ell_{II}$ and $\ell_2 = \ell_I$, where ℓ_I is monotonically decreasing with L from ℓ_c to ℓ_∞. The total compliance of the bar for this solution is

$$\mathsf{S}_{\mathrm{tot}}(L) = \frac{\mathsf{S}(\ell_I(L)) + \mathsf{S}(\ell_{II}(L))}{2}. \tag{30}$$

For long bars $(L \gg \ell_c)$, $\ell_I \to \ell_\infty$ and $\ell_{II} \to L - \ell_\infty$ constitutes a useful asymptotic approximation of the solution.

Figure 7-right compares the total compliance of the two solutions, which is inversely proportional to the corresponding elastic energy: their difference is immaterial in absolute value for the considered numerical example. This is related to the fact that the change of concavity of $S(\ell)$ is quantitatively very small and implies a small margin of stability of the solutions. This point will be discussed further in the Section 5 dedicated on the study of the influence of the geometric and material parameters and in the conclusions.

The results obtained with the modular approach are in agreement with the preliminary analysis of Section 3.1 obtained via direct numerical simulations. In turn, we can generalize the modular approach to treat the case with several cracks without further numerical burden.

4.2 General results for $n-1$ cracks dividing the bar in n segments

When the properties (P1-P3) in Section 3.3 are verified, there can be at most two distinct cell lengths ℓ_I and $\ell_{II} > \ell_I$ such that $\mathsf{S}'(\ell_I) = \mathsf{S}'(\ell_{II})$. Moreover, this is possible only for $\ell_{II} > \ell_c$, and $\mathsf{S}''(\ell_I) < 0$, $\mathsf{S}'(\ell_{II}) > 0$. This implies three fundamental consequences:

1. There can be at most two different elemental segment lengths ℓ_I and ℓ_{II} co-existing in a solution of the optimality conditions (15).
2. Because of the stability criterion (S2) in Section 3.2, stable solutions can have at most one long elemental cell length ℓ_{II}.
3. Applying the stability condition (S3) in Section 3.2, solutions with $n-1$ short segments and one long segment are stable if

$$r := \frac{1}{\mathsf{S}''(\ell_1^*)} + \frac{1}{\mathsf{S}''(\ell_n^*)} + \sum_{i=2}^{n-1} \frac{2}{\mathsf{S}''(\ell_i^*/2)} < 0. \tag{31}$$

We conclude that the possible solutions of the problem of Section 3.2 for a bar of length L divided in n segments by $n-1$ cracks can be classified as sketched in Figure 8:

(H) Homogeneous solutions with uniform cell lengths as in (18). These solutions are stable for

$$L < L_c = 2\,(n-1)\,\ell_c \tag{32}$$

and the corresponding total compliance is

$$\mathsf{S}_{\text{tot}}^{(H)}(\underline{\ell}) = (n-1)\,\mathsf{S}\left(\frac{L}{2\,(n-1)}\right). \tag{33}$$

(A) Solutions with one long cell of length ℓ_{II} and $n-1$ short cells of length $\ell_I(\ell_{II})$, where the long cell is placed in at one of the two ends of the bar. The corresponding total bar length and compliance are

$$L = (2\,n-3)\ell_I + \ell_{II}, \qquad \mathsf{S}_{\text{tot}}(\underline{\ell}) = \frac{2n-3}{2}\mathsf{S}(\ell_I) + \frac{\mathsf{S}(\ell_{II})}{2} \tag{34}$$

These solutions are stable for

$$-\frac{\mathsf{S}''(\ell_I)}{\mathsf{S}''(\ell_{II})} > 2n-3.$$

(B) For $n > 2$ we can consider non-homogenous solutions with one long cell of length ℓ_{II} and $n-1$ short cells of length $\ell_I(\ell_{II})$, with the long cell placed in any of the cell not at the boundary. The corresponding total bar length and compliance are

$$L = 2(n-2)\ell_I + 2\,\ell_{II}, \qquad \mathsf{S}_{\text{tot}}(\underline{\ell}) = (n-2)\mathsf{S}(\ell_I) + \mathsf{S}(\ell_{II}) \tag{35}$$

These solutions are stable for

$$-\frac{\mathsf{S}''(\ell_I)}{\mathsf{S}''(\ell_{II})} > n-1.$$

Given the above results, substituting $\ell_I(\ell_{II})$ in the equations (34) and (35) and solving them for ℓ_{II} as a function of L and n provides the lengths of short and long segments ℓ_I and ℓ_{II} as function of the total bar length and the number of segments. Figure 8-right plots the results for different n for the case of solutions of the type (B). The case (A) is qualitatively similar.
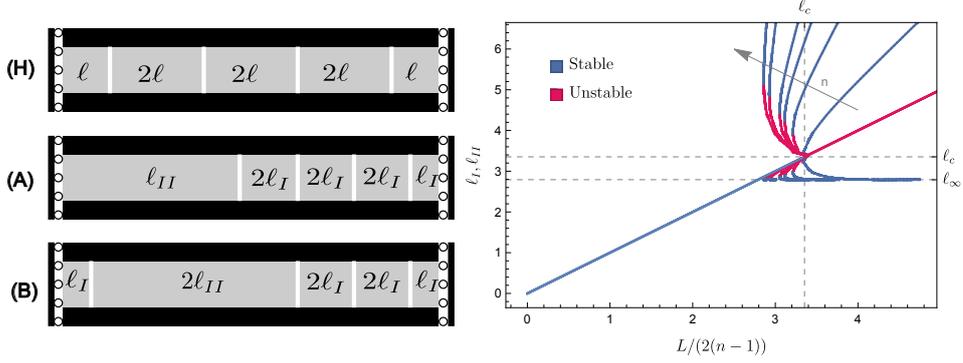
Fig. 8: Bar divided in $n > 2$ segments by $n - 1$ cracks. Left: Different kind of stable solutions for the case $n = 5$: homogeneous (H); long segment at the boundary (A); long segment not at the boundary (B). Right: Length of the short (ℓ_I) and long segment ℓ_{II} for the bar divided in two segments with stable solution in blue and unstable solutions in pink: possible solutions for different values of $n \geq 2$ are reported.

Remark 2 In the variant of the traction boundary conditions in Figure 3 the discussion is simpler. The critical total bar length for the stability of the homogeneous solution with $n - 1$ cracks is $L_n^{(c)} = 2\,n\,\ell_c$, there is no distinction between solutions of type (A) and (B) and the total bar length and elastic compliance for solutions with $n - 1$ short cells and one long cell are:

$$L = 2(n - 1)\ell_I + 2\,\ell_{II}, \qquad \mathsf{S}_{\text{tot}}(\underline{\ell}) = (n - 1)\mathsf{S}(\ell_I) + \mathsf{S}(\ell_{II}). \tag{36}$$

5 Effect of the material and geometric parameters

The stability of the solution with homogeneous crack spacing depends on the concavity property of the derivative of the compliance function of the basic cell $S(\ell)$. As shown in Figure 5, $S(\ell)$ is asymptotically linear for $\ell \to 0$ and $\ell \to \infty$. The change of concavity in the transition zone around $\ell = \ell_c$ is not clearly visible in the plot of $S(\ell)$. It is detected only by the change of sign of the slope of $S'(\ell)$ and the change of sign of $S''(\ell)$ in the diagrams of Figure 5. The ratio $S'(\ell_c)/S'(\infty)$ between the minimal value of S', attained at the critical length ℓ_c, and its value for $\ell \to \infty$ is a possible quantitative signature of this change of concavity. The previous sections reported the results for the specific example of a laminated bar made of isotropic materials with a stiffness ratio $E_o/E_c = 1$ and a thickness ratio $H_o/H_c = 0.5$. In this case, the change of concavity is real, but quantitatively very small, as shown by the values of $S'(\ell_c)$ and $S'(\infty)$ in Figure 5. This implies that the margin of stability of the solutions is small, as discussed also in the comments to Figure 7. We investigate here how this change of concavity varies with the material and geometrical parameters.

Figure 9 illustrates the results obtained when varying the thickness (left column) and stiffness ratios (right column) for the case of isotropic materials with $\nu = 0.3$. They have been obtained with the numerical method described in Section 3.3. Each curve is the outcome of an interpolation of 100 finite element computations for different values of the bar length, keeping constant the other parameters. We managed to reliably investigate numerically only stiffness and thickness ratio of the order of $0.1 - 10$, the numerical problem becoming ill-conditioned otherwise. The
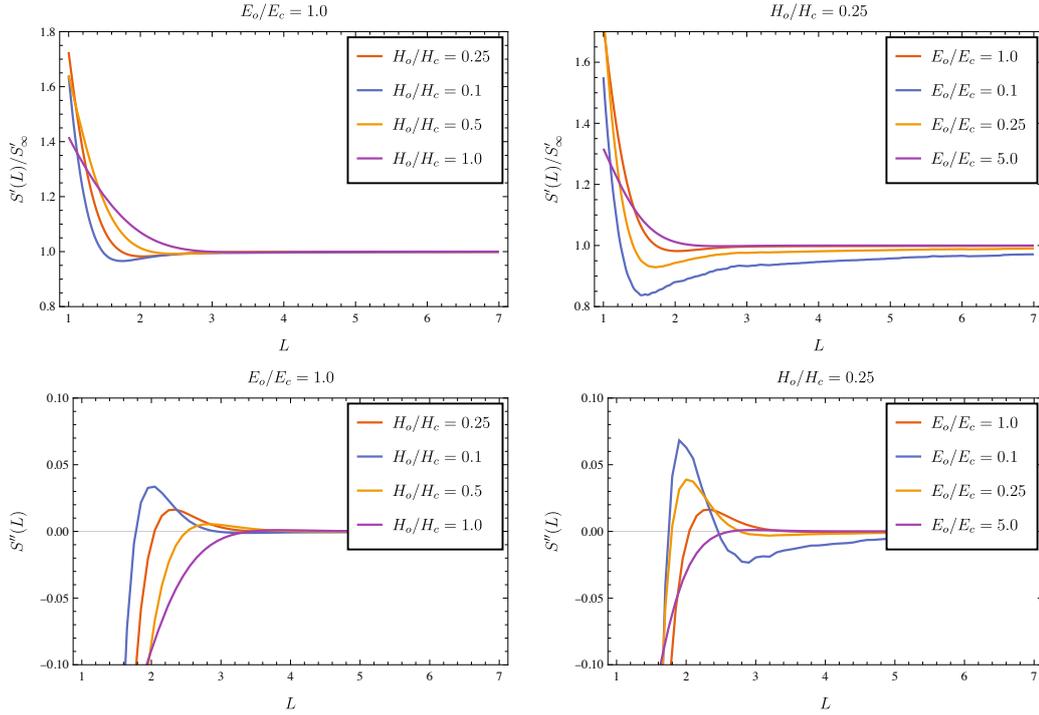
Fig. 9: Dependence of derivatives of the compliance of the basic module on the material and geometric parameters. The numerical results for the first ($S'(L)$, top row) and second ($S''(L)$, bottom row) derivatives for different thickness (left column) and stiffness ratios (right column) are obtained with the method of Section 3.3. Results for isotropic materials with $\nu = 0.3$.

small scale oscillations of the curves of S' and S'' for $H_o/H_c = 0.1$ and $E_o/E_x = 0.1$ are a marker of such numerical issues.

We observe the following facts:

– The ratio $S'(\ell_c)/S'(\infty)$ is larger for small stiffness ratios and small thickness ratios, *i.e.* soft and thin outer layers. For $H_o/H_c = 0.1$ and $E_o/E_x = 0.1$ this ratio is of the order of the unity.
– The value of ℓ_c for which the minimum of S' is attained varies almost linearly with the thickness of the outer layer, while its dependence on the stiffness ratio is very weak.

Figure 10 reports the curve of $S'(\ell)$ for the case of $[0/90/0]$ composite laminates made of unidirectional fiber reinforced materials. We consider typical carbon (left) and glass (right) fiber composites with different thickness ratios, see the caption for the specific material parameters. The change of slope is either absent of barely visible for all the cases. As in the isotropic case, it is more evident for small thickness ratios. This can be explained by the high stiffness ratio between 0 and 90 laminae which is of the order 4 and 10 for the glass and carbon composites, respectively. Figure 11 illustrates the role of the shear stiffness for the case of glass fibers. The ratio $S'(\ell_c)/S'(\infty)$ increases with increasing shear stiffness. The small values of the shear stiffness of fiber-reinforced composites is a possible explanation of the difference with respect to the isotropic case of Figure 9.
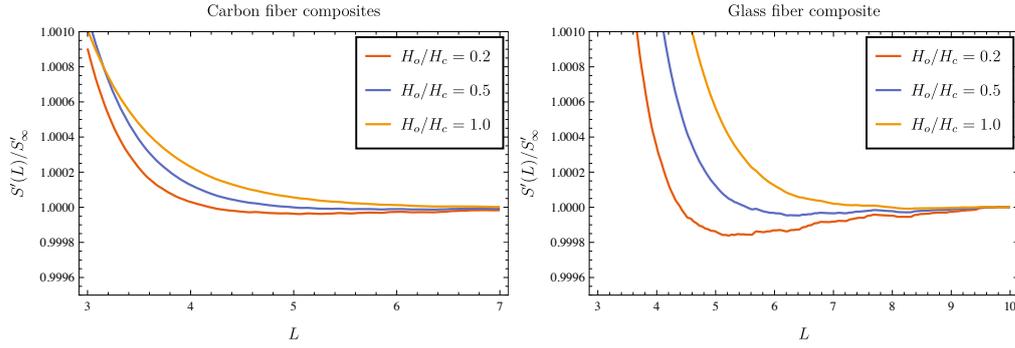
Fig. 10: Basic module compliance derivative $S'(L)$ for $0/90/0$ composite laminate made of typical Glass Fiber laminae ($E_x = 43.5$ GPa, $E_y = 11.5$ GPa, $G_{xy} = 3.45$ GPa, $\nu_{xy} = 0.25$) or typical carbon fiber laminae ($E_x = 132$ GPa, $E_y = 10.8$ GPa, $G_{xy} = 5.65$ GPa, $\nu_{xy} = 0.24$). The results are for different thickness ratios.
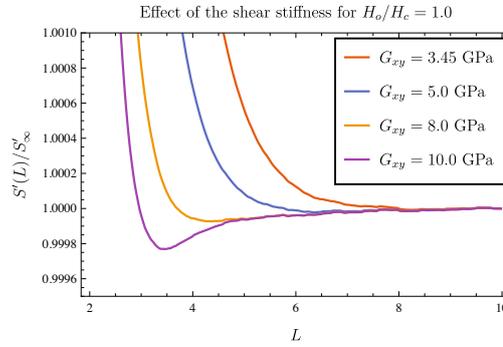

Fig. 11: Influence of the shear stiffness G_{xy} on the derivative of the compliance of the basic module. The results are a $0/90/0$ composite laminate made of an ideal material with $E_x = 43.5$ GPa, $E_y = 11.5$ Gpa, $G_{xy} = 3.45$ GPa, $\nu_x y = 0.25$ and varying G_{xy}.

6 Optimal number of cracks

Our work focuses on the study of the crack spacing for a given number of cracks. We quickly sketch here how to determine the optimal number of cracks as a function of the loading. For the sake of conciseness, we limit the discussion to the case of uniform crack spacing and the simplified boundary conditions in Figure 3-bottom. For this case, the total Griffith energy of the bar of total length L with n cracks writes as:

$$\mathsf{F}_n = \frac{1}{2\,n\,\mathsf{S}\left(\frac{L}{2n}\right)} \frac{\bar{u}^2}{2} + G_c(n-1) \tag{37}$$

Figure 12-left reports the plots of F_n for $n = 1, \ldots, 10$ and $L = 10$. According to the global energy minimization principle, the cracked stated is the one with minimal energy. The critical load $\bar{u}_n$ to pass from $n-1$ to n cracks is simply obtained by imposing $F_n = F_{n+1}$. The grid lines and the black points in Figure 12 mark these critical loadings. Physically, the number of segments n is a discrete variable taking integer values. In a smeared model, one can also regard n as a real number, approximate indicator of the damage level in the core. In this setting, it is
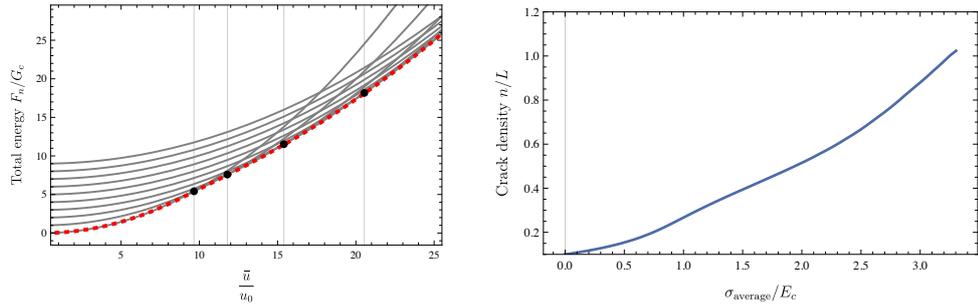
Fig. 12: Left: Total energy F_n (37) for different number of cracks, where the displacement is scaled with $u_0 = \frac{G_c}{E_c H_c}$. The grid lines and the black dots denote the critical loadings for which $F_n = F_n + 1$. The dashed red curve is F_{n^*} with n^* such that $dF_n/dn = 0$, which gives an approximation of the lower envelop of the F_n's. Right: crack density as a function of the average stress in the bar corresponding to the red lower envelope in the left plot.

possible to get the optimal n by solving the equation $dF_n/dn = 0$. This gives the red dashed curve in Figure 12-left, which is an excellent approximation of the lower envelop of the F_n curves, and the plot in Figure 12-right for the crack density n/L as a function of the average stress in the bar $\sigma_{\text{average}} = \bar{u}/\left(2\,n\,\mathsf{S}(L/2n)\right)$.

Previous works have shown similar results to be in agreement with experimental findings even with uniform crack spacing hypothesis (see e.g. Berthelot, 2003; Nairn, 2000). Figure 13 further provides a state diagram showing the optimal number of segments (hence cracks) as a function of the loading and the bar length.

The energy gap between solution with uniform and non-uniform spacing is generally low for the numerical case tested in this paper. Hence, considering non-uniform crack spacing does not significantly influence the results for the optimal number of cracks. For this reason, we do not report results for non-uniform spacing. The effect of the crack irreversibility is a further point that we do not address here in details. During a quasi-static evolution, not all the cracked states of Figures 12 are accessible, because previously created cracks cannot heal. León Baldelli et al., 2011 reports similar results for the case of a one-dimensional model of a bar-substrate system. The discussion is not duplicated here.

7 Conclusion

We have studied transverse fracture in the core layer of symmetric laminate composites using a sharp interface Griffith model and a variational approach. We have shown that, even in perfect systems, the solution with uniform crack spacing, commonly accepted in the literature, is not always optimal. For sufficiently long bars, solutions with uniform spacing becomes unstable and stable solutions with a non-uniform crack spacing appear. With a modular model, we have related the bifurcation phenomenon to the concavity properties of the compliance $S(\ell)$ of the basic cell of the system as a function of the cell length ℓ, applying the ideas of Bourdin et al., 2008. The change of concavity of the elementary cell compliance is a necessary condition for the existence of solutions with non-uniform crack spacing. We computed $S(\ell)$ and its first and second derivatives numerically by finite element method and an accurate domain derivative approach. Our results indicate a change of concavity of S', related to the instability of the solution with uniform crack spacing. For the case of bar with n cracks, we have shown that the two values of cell lengths are possible, short and long, and that only solution with a single long cell are stable.
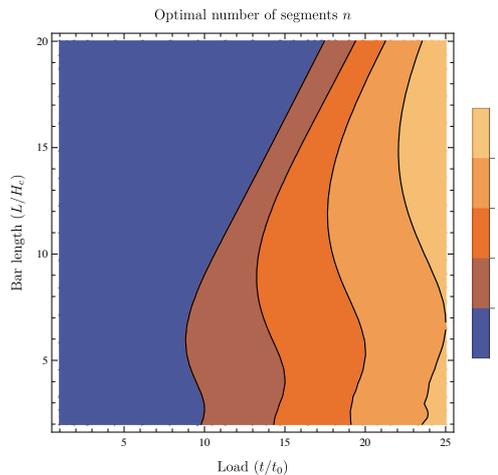
Optimal number of segments n

Fig. 13: Optimal number of segments n, as a function of the loading and the bar length, where n segments correspond to $n - 1$ cracks.

Our results unveil a novel phenomenon in perfect symmetric laminated composites and describe its main qualitatively properties: the bifurcation from solutions with uniform crack spacing to non-uniformly spaced solutions. However, the stability margin of the different solutions turns out to be quantitatively small. For usual material and geometric parameters, the dependency of the total energy of the laminate on the crack spacing is very weak, until the elementary cell length reaches a critical length of the order of the thickness. This implies that solutions with the same crack number and different crack spacing are almost equivalent from the energetic point of view. In particular, the change of concavity of the elemental compliance S is barely visible or absent for classical [0/90/0] composite laminates with unidirectional laminae made of fiber reinforced materials with large stiffness ratio and a relatively low shear stiffness. In common situations, imperfections play a fundamental role and cannot be neglected. In particular, the influence of defects in initiating transverse cracks is stronger in the early stage of the multiple cracking process. In these contexts, our approach cannot replace finer models considering the effect of random or deterministic defects to predict the crack spacings (see e.g. Silberschmidt, 2005; Vinogradov and Hashin, 2005). Yet, the results of our dedicated parametric analysis indicate that the change of concavity of S, related to energetic gap between solutions with uniform and non-uniform crack spacing, becomes of the order of unit for composite laminates with thin and soft outer layers. We hope that our work can instigate further experimental works to understand whether the competition between uniform and non-uniform crack spacing can be deterministically linked to the geometrical and material properties in this specific regime, as predicted by our analysis. From the theoretical and numerical perspective, multiple cracks in layered composites has been recently studied with cohesive (Javaland et al., 2012) and phase-field fracture models (Bleyer and Alessi, 2018; León Baldelli et al., 2014; Quintanas-Corominas et al., 2019). Investigating the crack spacing issue in these contexts is a further interesting perspective that we are currently pursuing. Our model neglects delamination cracks, that play an important role in the determining the minimal crack spacing for high crack densities (Berthelot and Corre, 2000). Their effect can be included in the variational framework as in León Baldelli et al., 2011 or Bleyer and Alessi, 2018.

Acknowledgement

References

Alnæs, M. S., A. Logg, K. B. Ølgaard, M. E. Rognes, and G. N. Wells (2014). "Unified Form Language: A Domain-Specific Language for Weak Formulations of Partial Differential Equations". In: 40.2.

Berthelot, J. (2003). "Transverse Cracking and Delamination in Cross-Ply Glass-Fiber and Carbon-Fiber Reinforced Plastic Laminates: Static and Fatigue Loading". In: *Applied Mechanics Reviews* 56, pp. 111–147.

Berthelot, J.-M. and J.-F. L. Corre (2000). "Statistical Analysis of the Progression of Transverse Cracking and Delamination in Cross-Ply Laminates". In: *Composites Science and Technology* 60.14, pp. 2659–2669.

Berthelot, J.-M., P. Leblond, A. El Mahi, and J.-F. Le Corre (1996). "Transverse Cracking of Cross-Ply Laminates: Part 1. Analysis". In: *Composites Part A: Applied Science and Manufacturing* 27.10, pp. 989–1001.

Bleyer, J. and R. Alessi (2018). "Phase-Field Modeling of Anisotropic Brittle Fracture Including Several Damage Mechanisms". In: *Computer Methods in Applied Mechanics and Engineering* 336.

Bourdin, B., G. A. Francfort, and J.-J. Marigo (2008). "The Variational Approach to Fracture". In: *Journal of Elasticity* 91.1-3, pp. 5–148.

Dvorak, G. J. and N. Laws (1, 1986). "Analysis of First Ply Failure in Composite Laminates". In: *Engineering Fracture Mechanics* 25.5, pp. 763–770.

Francfort, G. and J.-J. Marigo (1998). "Revisiting Brittle Fracture as an Energy Minimization Problem". In: *Journal of The Mechanics and Physics of Solids* 46.

García, I. G., V. Mantič, A. Blázquez, and F. París (1, 2014). "Transverse Crack Onset and Growth in Cross-Ply [0/90]s Laminates under Tension. Application of a Coupled Stress and Energy Criterion". In: *International Journal of Solids and Structures* 51.23, pp. 3844–3856.

Hashin, Z. (1985). "Analysis of Cracked Laminates: A Variational Approach". In: *Mechanics of Materials* 4.2, pp. 121–136.

Javaland, M., H. Hosseini-Toudeshky, and B. Mohammadi (2012). "Numerical Modeling of Diffuse Transverse Cracks and Induced Delamination Using Cohesive Elements." In: *Proc Instit Mech Eng C: J Mech Eng Sci*.

Leguillon, D. (2002). "Strength or Toughness? A Criterion for Crack Onset at a Notch". In: *European Journal of Mechanics - A/Solids* 21.1, pp. 61–72.

León Baldelli, A. A., J.-F. Babadjian, B. Bourdin, D. Henao, and C. Maurini (2014). "A Variational Model for Fracture and Debonding of Thin Films under In-Plane Loadings". In: *Journal of the Mechanics and Physics of Solids* 70, pp. 320–348.

León Baldelli, A. A., B. Bourdin, J.-J. Marigo, and C. Maurini (2011). "Fracture and Debonding of a Thin Film on a Stiff Substrate: Analytical and Numerical Solutions of a One-Dimensional Variational Model". In: *Continuum Mechanics and Thermodynamics* 25.

Luenberger, D. (2008). "Linear and Nonlinear Programming". In.

Maimí, P., H. Rodríguez, N. Blanco, and J. Mayugo (2015). "Numerical Modeling of Matrix Cracking and Intralaminar Failure in Advanced Composite Materials". In: *Numerical Modelling of Failure in Advanced Composite Materials*. Elsevier, pp. 175–192.

Manders, P., T. Chou, F. Jones, and J. Rock (1983). "Statistical Analysis of Multiple Fracture in [0/90/0] Glass Fiber/Epoxy Resin Laminates". In: *J. Mater. Sci.* 19, pp. 2876–2889.

Nairn, J. (2000). "Matrix Microcracking in Composites". In: *Comprehensive Composite Materials*. Ed. by A. Kelly and C. Zweben. Vol. 2. Oxford: Pergamon, pp. 403–432.

Okabe, T., M. Nishikawa, and N. Takeda (2008). "Numerical Modeling of Progressive Damage in Fiber Reinforced Plastic Cross-Ply Laminates". In: *Composites Science and Technology* 68.10, pp. 2282–2289.

Parvizi, A. and J. Bailey (1978). "Constrained Cracking in Glass Fibre Reinforced Epoxy Cross-Ply Laminates". In: *Journal of Materials Science* 13, pp. 195–210.

Puglisi, G. and L. Truskinovsky (2000). "Mechanics of a Discrete Chain with Bi-Stable Elements". In: *Journal of the Mechanics and Physics of Solids* 48.1, pp. 1–27.

Quintanas-Corominas, A., J. Reinoso, E. Casoni, A. Turon, and J. A. Mayugo (15, 2019). "A Phase Field Approach to Simulate Intralaminar and Translaminar Fracture in Long Fiber Composite Materials". In: *Composite Structures* 220, pp. 899–911.

Scroggs, M. W., J. S. Dokken, C. N. Richardson, and G. N. Wells (2022). "Construction of Arbitrary Order Finite Element Degree-of-Freedom Maps on Polygonal and Polyhedral Cell Meshes". In: 48.2.

Silberschmidt, V. (2005). "Matrix Cracking in Cross-Ply Laminates: Effect of Randomness". In: *Composites Part A: Applied Science and Manufacturing* 36.2, pp. 129–135.

Vinogradov, V. and Z. Hashin (2005). "Probabilistic Energy Based Model for Prediction of Transverse Cracking in Cross-Ply Laminates". In: *International Journal of Solids and Structures* 42.2, pp. 365–392.